Complex monoclinic superstructure in Sr-IV

T. Bovornratanaraks,[1,2] D. R. Allan,[1] S. A. Belmonte,[1] M. I. McMahon,[1] and R. J. Nelmes[1]
[1]*SUPA, School of Physics and Centre for Science at Extreme Conditions, The University of Edinburgh, Mayfield Road, Edinburgh EH9 3JZ, United Kingdom*
[2]*Department of Physics, Faculty of Science, Chulalongkorn University, Bangkok, 10330, Thailand*
(Received 28 July 2005; revised manuscript received 20 September 2005; published 20 April 2006)

The complex structural behavior of strontium under high pressure has been studied using angle-dispersive x-ray powder-diffraction techniques. The previously unknown structure of Sr-IV is found to be monoclinic, with space group *Ia* and 12 atoms per unit cell, and is a helical distortion of the β-tin structure of Sr-III. This structure has not been observed before in an element Sr-IV is stable from 37.7(2) GPa to 46.3(3) GPa where it transforms to the composite incommensurate Sr-V phase. Diffraction patterns over the small range from 36.0 to 37.7 GPa cannot be fitted completely by either Sr-III or Sr-IV. The previously identified minority phase of unknown structure that appears at the Sr-II to Sr-III transition persists through Sr-IV and Sr-V.

DOI: 10.1103/PhysRevB.73.144112 PACS number(s): 61.50.Ks, 62.50.+p

The alkali and alkaline-earth elements exhibit a rich variety of high-pressure crystalline phases under pressure, accompanying $s \rightarrow d$ electron transfer.[1] Despite much experimental and theoretical interest in this phenomenon, the crystal structures of many of the high-pressure phases of these elements have long resisted all attempts at solution. However, the development of angle-dispersive diffraction techniques coupled with monochromatic synchrotron radiation has recently led to the determination of the high-pressure structures of Li-III,[2] Na-II,[3] Rb-III,[4] Rb-IV,[5] Rb-VI,[6] Cs-III,[7] Cs-V,[8] Sr-III,[9] Sr-V,[10] and Ba-IV.[11] The structures of most of these phases are remarkably complex, and this is particularly true of Ba-IV, Sr-V, and Rb-IV, where the structures comprise two interpenetrating components—a host and a guest—that are incommensurate with each other along their common *c* axis.

The recent solutions to the structures of Sr-III (Ref. 9) and Sr-V (Ref. 10) leaves Sr-IV—stable between ~38 GPa and ~49 GPa—as the only reported high-pressure phase of an alkaline-earth metal whose structure remains unknown. In this paper we report a solution to Sr-IV as a monoclinic superstructure of the Sr-III (β-tin) structure. This structure type has not been observed previously in an element. Rietveld refinement reveals that the distortions of Sr-IV from the β-tin structure can be modeled using a single displacement parameter.

Strontium of 99.968% stated purity was obtained from Johnson Matthey and The Aldrich Chemical Company in the form of vacuum distilled granules. Samples of a suitable size were prepared under mineral oil and then loaded into either Diacell DXR5 or DXR6 diamond-anvil cells.[12] The mineral oil used was light white mineral oil purchased from The Aldrich Chemical Company, which was dried prior to use by contact with freshly cut potassium metal. This mineral oil was also used as a pressure-transmitting medium to prevent oxidation and to provide a quasihydrostatic pressure medium. The pressure was measured with the ruby fluorescence technique.[13] Diffraction data were collected on station 9.1 at the Synchrotron Radiation Source (SRS), Daresbury Laboratory, using a wavelength of 0.4654 Å,[14] and on beamline ID09 at the European Synchrotron Radiation Facility (ESRF), Grenoble,[15] using a wavelength of 0.45115 Å. The resulting two-dimensional images were integrated azimuthally using EDIPUS (Ref. 14) for the SRS data and FIT2D (Ref. 16) for the ESRF data, to produce conventional one-dimensional powder patterns. Rietveld refinement of the integrated profiles was performed using GSAS.[17]

On pressure increase, the Sr-I (face-centered cubic) to Sr-II (body-centered cubic) and the Sr-II to Sr-III transitions were observed at 3.5 GPa and 25 GPa, respectively, in agreement with earlier studies.[18] As reported previously,[9] diffraction patterns in the Sr-III stability range exhibit textured Debye-Scherrer (DS) rings arising from Sr-III, which can be well fitted with the (β-tin) structure, and smooth DS rings from an additional phase. This additional phase was also observed by Winzenick and Holzapfel,[19] but was not identified as such, leading to an incorrect solution for the Sr-III structure. The structure of the smooth additional phase is, as yet, unknown, and we will refer to it as the *S* phase.

Sr-III diffraction patterns were observed to 36.0(2) GPa, at which point two new diffraction peaks appeared at 9.4° and 11.3°, as marked by asterisks in inset (b) of Fig. 1. With further increase in pressure, the higher-angle of these two peaks splits, while the lower-angle peak first moves to a *smaller* Bragg angle (longer *d* spacing) before, at 37.7(2) GPa, becoming a doublet. Further increases in pressure lead to an increased splitting of this doublet and a splitting of many of the other diffraction peaks, until, at 46.3(3) GPa, diffraction peaks from Sr-V are observed. Peaks of the *S* phase, the strongest of which are indicated by arrows in inset (b) of Fig. 1, show no changes over this pressure range and persist through the Sr-IV to Sr-V transition.

The apparent relationship between the Sr-III and Sr-IV diffraction patterns suggest that the two structures are related. It is to be noted that while many of the Sr-III peaks split into two or more peaks in Sr-IV (Fig. 1), the (200) and (020) reflections of Sr-III continue to overlap as a singlet over the entire stability range of Sr-IV [inset (a) of Fig. 1]. The *d* spacings of the corresponding reflections in Sr-IV

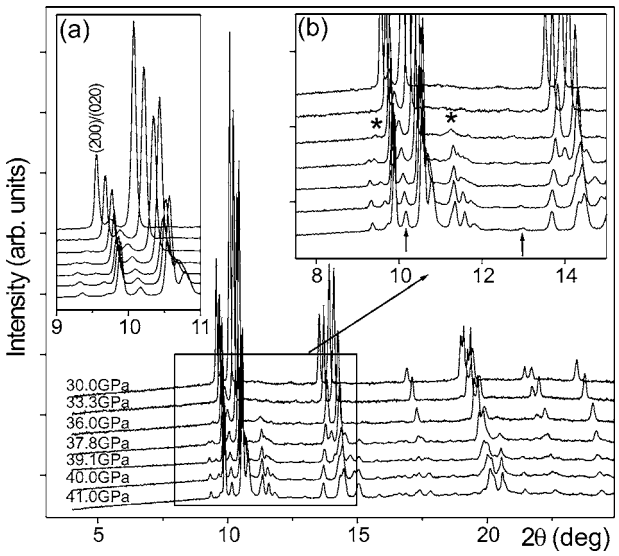

FIG. 1. Diffraction profiles from Sr collected between 30 GPa and 41 GPa, showing the evolution of Sr-III into Sr-IV. Inset (a): enlargement of the most intense peaks in the profiles. The (200)/(020) peak from Sr-III, which remains a singlet in Sr-IV, is identified. Inset (b): enlargement of the low-angle part of the profiles. The asterisks in the 36 GPa profile mark the two peaks observed in the pressure range between pure Sr-III and pure Sr-IV, as discussed in the text. The two peaks marked by arrows in the 41 GPa profile identify the two strongest peaks from the unknown (*S*) phase reported previously.

must therefore remain equal at all pressures. *Ab initio* indexing using DICVOL (Ref. 20) revealed that Sr-IV can be indexed on a monoclinic unit cell with $a=5.745$ Å, $b=7.801$ Å, $c=5.536$ Å, and $\beta=97.01°$ at 41.7(3) GPa. This unit cell is closely related to that of Sr-III, with $\vec{a}_{IV}=-\frac{1}{2}\vec{a}+\frac{1}{2}\vec{b}+\frac{3}{2}\vec{c}$, $\vec{b}_{IV}=\vec{a}+\vec{b}$, and $\vec{c}_{IV}=-\frac{1}{2}\vec{a}+\frac{1}{2}\vec{b}-\frac{3}{2}\vec{c}$, without the monoclinic distortion to $a\neq c$. This relationship is illustrated in Fig. 2, and accounts for the nonsplitting of the (200) and (020) Sr-III reflections when they become the $(\bar{1}2\bar{1})$ and (121) reflections in Sr-IV: these reflections are symmetry related by the monoclinic twofold axis.

The volume of the Sr-IV unit cell is three times that of the tetragonal Sr-III cell and therefore contains 12 atoms. The

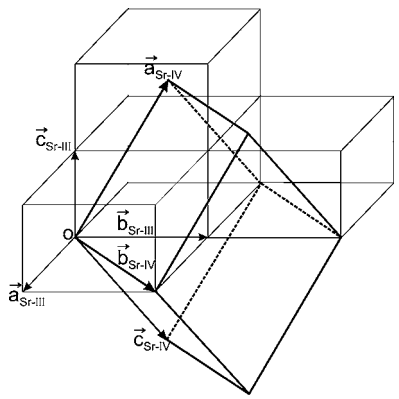

FIG. 2. Relationship between the unit cells of the Sr-III phase (light lines) and the superstructure Sr-IV phase (heavy lines).

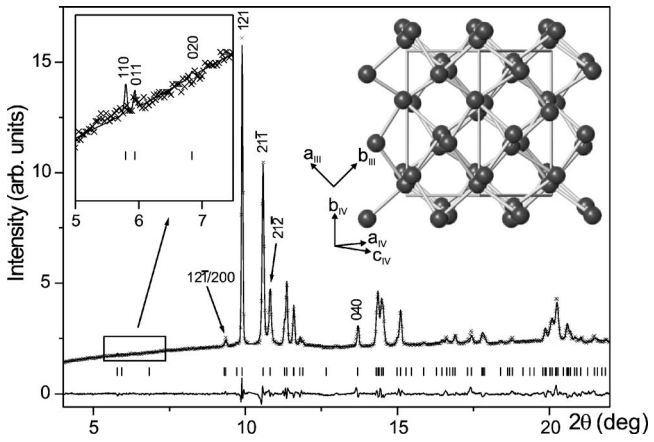

FIG. 3. Free (unconstrained) Rietveld refinement of Sr-IV at 41.7(3) GPa. Tick marks below the profile show the calculated peak positions, and the difference between the observed (crosses) and calculated (line) profiles is shown under the tick marks. The refined Sr-IV structure is shown viewed along the *c*-axis direction of the Sr-III structure, revealing the helical distortion along this direction. Inset: enlarged view of the fit to the very weak (110), (011), and (020) reflections.

Sr-IV diffraction profiles showed systematic absences compatible with two different space groups: *Ia* and *I*2/*a*. However, *I*2/*a* symmetry is not compatible with a β-tin-like structure. So the Sr-III structure was transformed into the non-centrosymmetric *Ia* unit cell to provide a probable initial model for Rietveld refinement, with the three independent atoms, Sr1, Sr2, and Sr3 placed on the 4*a* sites of *Ia* at $(\frac{1}{3},\frac{1}{8},\frac{2}{3})$, $(\frac{1}{2},\frac{5}{8},\frac{1}{2})$, and $(\frac{2}{3},\frac{1}{8},\frac{1}{3})$, respectively. Free refinement from these initial positions using GSAS converged to an excellent fit ($R_{wp}=0.0237$) to the whole pattern; as shown in Fig. 3. At 41.7 GPa, the final refined lattice parameters were $a=5.7456(2)$ Å, $b=7.8009(2)$ Å, $c=5.5370(3)$ Å, and $\beta=96.990(2)°$, with Sr1 at [0.3039(13), 0.1574(11), 0.6322(21)], Sr2 at [0.4787(17), 0.5784(7), 0.4645(36)], and Sr3 at [0.6840(8), 0.1445(11), 0.3459(19)].

The refined structure is shown in the inset to Fig. 3. As indicated, the drawing is viewed along the $[\bar{1}01]$ direction of the Sr-IV unit cell, and this coincides with the *c* axis of Sr-III. The displacements of Sr1, Sr2, and Sr3 from the positions they occupy in the β-tin Sr-III structure are in directions that lie in the Sr-III *a*-*b* plane and are approximately 120° apart (to within 5°). They thus form helical chains directed along the former Sr-III *c* axis, and the repeat distance of the structure along this direction is consequentially tripled to form a superstructure. Although satisfactory free refinements could be performed over the entire stability range of Sr-IV, the complexity of the structure, and the texture that was evident in the Sr-IV diffraction patterns, resulted in a scatter in the refined atomic coordinates of ~0.07—some 50–70 times larger than the estimated standard deviations of each point. We therefore tested the use of structural constraints, suggested by the almost regular helical distortion, to reduce the number of refinable atomic parameters.

Constraints on the structure beyond those imposed by the space-group symmetry are also indicated by the fact that the

three low-angle (110), (011), and (020) reflections of Sr-IV (see Fig. 3) are absent, or extremely weak, in all of the data collected at SRS over the entire stability range of Sr-IV. (These reflections are not required to be absent by the *Ia* symmetry.) With the much higher beam intensity of the ESRF, it was found that the (011) reflection was just discernible, but the (110) and (020) reflections were still not visible, even in long-exposure patterns in which the strongest peaks oversaturated the image plate (see the observed profile in inset (a) of Fig. 4). The free refinements put intensities in these reflections different from the observations—as shown, for example, in the inset to Fig. 3 where there is significant calculated intensity in the (110) reflection.

Three different models were tested in the constrained refinements. In each, the nine independent atomic coordinates (x,y,z for Sr1, Sr2, and Sr3) were related to a single refinable displacement parameter D in a way that allowed the atoms to displace in consecutive layers parallel to the $(\bar{1}01)$ plane and in directions 120° apart in that plane. The three models differ in having one of the directions along the monoclinic b axis in the first,[21] along the normal to the monoclinic b axis in the second,[22] and along the β-tin a axis (Ref. 23) in the third. In each model, D is the (fractional) displacement of an atom from its transformed β-tin fractional coordinates. In the case of atom Sr1 in model (i), this displacement is along the monoclinic b axis (Ref. 21), and the magnitude of the displacement is thus $\Delta = D \times b(\text{Å})$. The relations in Refs. 21–23 are used to refine D and, in all three models, place Sr1, Sr2, and Sr3 in a helical arrangement on the surface of a cylinder of radius $D \times b$, or $\Delta(\text{Å})$. The axis of the helix, along $[\bar{1}01]$, is slightly inclined to the $(\bar{1}01)$ plane because of the (small) difference in magnitude between the a and c lattice parameters, and so the atoms are constrained to displace not quite perpendicular to the helix axis. But since the displacements deviate at most only 3.5° from perpendicular, the constraint to lie in the $(\bar{1}01)$ plane is a good approximation.

Rietveld refinements performed with each of the models showed that although the imposed constraints ensured that the (110), (011), and (020) reflections were calculated to be weak in all cases, only model (iii) gave a really good fit. Figure 4 shows the Rietveld refinement of data collected at 41.7(3) GPa, using constrained model (iii), and the inset (a) shows the agreement between the low-angle (ESRF) data and the calculated profile for this model. While model (iii) is in accord with the data in putting the strongest intensity in the (011) reflection, as shown, models (i) and (ii) both put the strongest intensity in the (110) reflection. (Note that these features are all too small to see at all on the scale of the main figure.)

The lattice parameters from this constrained Rietveld refinement at 41.7(3) GPa are $a=5.7463(2)$ Å, $b=7.8013(3)$ Å, $c=5.5360(4)$ Å, and $\beta=96.986(3)°$, with three refinable atoms Sr1 [0.3031(2), 0.1545(3), 0.6353(3)], Sr2 [0.4889(1), 0.5847(4), 0.4885(1)], Sr3 [0.7079(4), 0.1358(1), 0.3762(4)] with $D=0.0417$ (4) and $R_{wp}=0.0303$. Rietveld refinements using this single parameter model were performed over the full stability range of Sr-IV and were found to give an excellent fit at all pressures. The resulting

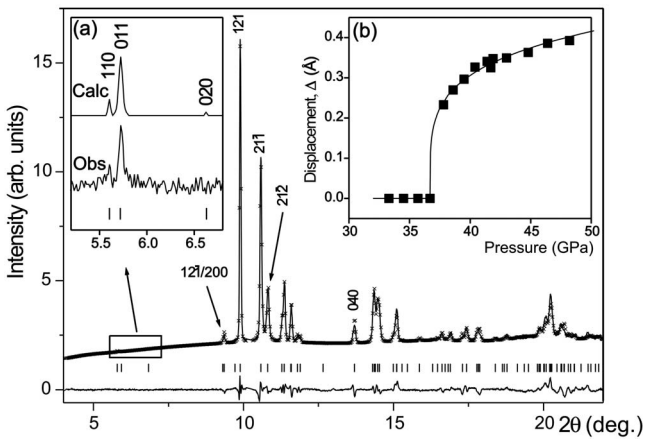

FIG. 4. Constrained Rietveld refinement of Sr-IV at 41.7(3) GPa with model (iii) (see text). The tick marks and difference profile are shown as in Fig. 3. Inset (a): ESRF data for the range marked, compared with the calculated profile for constrained model (iii). Note that this inset is not an enlargement of the main profile fit, which uses the same SRS data as Fig. 3. Inset (b): pressure dependence of the helical displacement Δ as obtained from the constrained refinements (see text). The estimated errors are approximately the same as the size of the symbols. The line through the points is a guide to the eye.

values of the displacement Δ vary smoothly with pressure, as shown in the inset (b) to Fig. 4. The refined lattice parameters as a function of pressure are given in Table I.

Although the *Ia* structure provides an excellent fit to the Sr-IV data over the full range from 37.7 GPa to 46.3 GPa, it does not account for the low-angle reflection first observed at 36 GPa (Fig. 1), nor its movement to longer d spacing with increasing pressure. Only after this reflection has transformed to a doublet at 37.7(2) GPa are the positions of all observed peaks accounted for. It would thus appear that there is a previously unreported intermediate or additional minority phase appearing in this narrow pressure range. Extensive attempts to index diffraction patterns collected between

TABLE I. Refined lattice parameters and the helical displacement Δ as a function of pressure for Sr-IV, using constrained model (iii).

Pressure (GPa)	a (Å)	b (Å)	c (Å)	β (°)	Δ (Å)
37.8	5.7952(3)	7.7599(4)	5.7141(7)	97.090(5)	0.233(3)
38.6	5.7896(6)	7.7821(5)	5.6584(3)	97.069(3)	0.270(3)
39.5	5.7753(2)	7.7903(5)	5.6124(6)	96.970(5)	0.296(3)
40.4	5.7715(3)	7.8103(6)	5.5724(6)	97.139(4)	0.327(3)
41.4	5.7483(8)	7.8051(6)	5.5317(4)	96.950(2)	0.341(3)
41.7	5.7463(2)	7.8013(3)	5.5360(4)	96.986(3)	0.325(3)
41.9	5.7247(3)	7.8044(6)	5.4798(7)	96.958(5)	0.347(3)
43.0	5.7108(5)	7.7956(14)	5.4654(10)	96.979(10)	0.349(3)
44.8	5.6861(2)	7.7987(3)	5.4128(4)	97.058(3)	0.363(3)
46.4	5.6502(2)	7.7802(4)	5.3593(6)	97.015(4)	0.386(4)
48.2	5.6211(7)	7.7964(6)	5.3106(5)	97.010(12)	0.392(5)

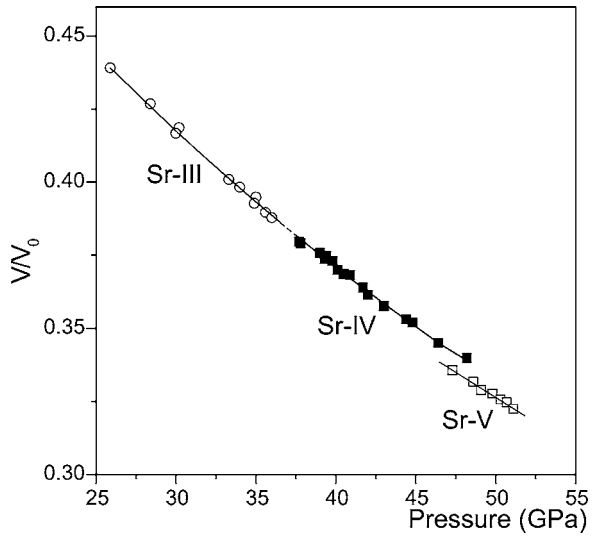

FIG. 5. V/V_0 for Sr-III, Sr-IV, and Sr-V, where V is the atomic volume and V_0 is its value in Sr-I at ambient pressure. The lines through the data are guides for the eye. No data points are plotted between 36.0 and 37.7 GPa, the range where there are additional unexplained peaks (see text).

36.0 GPa and 37.7 GPa have been unsuccessful.

This behavior possibly relates to the other unsolved minority phase—the smooth *S* phase that first appears at the transition from Sr-II to Sr-III. Because this is not present in Sr-I and Sr-II, and is always found in our data and in other studies,[9,19] we believe the *S* phase has to be another form of Sr rather than any form of impurity. This phase is stable through Sr-III and Sr-IV and into the stability field of Sr-V, where it transforms at 57 GPa into another accompanying phase that persists to at least 75 GPa.[10]

The equation of state of the phases of Sr between 26 and 52 GPa is shown in Fig. 5 in terms of V/V_0 (see Fig. 5 caption), excluding the *S* phase and the possible additional phase in the 36.0–37.7 GPa range. There is no measurable discontinuity between Sr-III and Sr-IV. The fact that the onset of the structural displacement in Sr-IV fits a curve falling continuously to zero [inset (b) of Fig. 4] suggests a continuous transition from Sr-III to Sr-IV, which would be in keeping with a lack of any volume discontinuity between these phases. However, the possible existence of an intermediate phase between Sr-III and Sr-IV, and the apparently discontinuous change in the diffraction pattern at the transition, provide evidence to the contrary. The behavior between 36.0 and 37.7 GPa needs to be clarified before this issue can be resolved.

In conclusion, the structure of Sr-IV, stable between 37.7(2) GPa and 46.3(3) GPa, is monoclinic, space group *Ia*, with 12 atoms per unit cell, and is a monoclinic distortion of the tetragonal β-tin structure of Sr-III. The distortion creates a superstructure characterized by helical chains that triple the lattice repeat along the direction of the β-tin *c* axis and this structure type has not been observed previously in any element. We have applied a constrained structural model with only a single refinable atomic coordinate, in which atoms displace from their β-tin positions in directions 120° apart in the $(\bar{1}01)$ plane, and find that this provides an excellent fit to Sr-IV over its entire stability range. For a complete understanding of the high-pressure phases of Sr, it remains yet to determine the structure and stability of the smooth *S* phase, and to clarify the phase behavior observed in the narrow 36.0 to 37.7 GPa range between pure Sr-III and pure Sr-IV.

We thank M. Hanfland of the ESRF and M. A. Roberts and A. A. Neild of the SRS for their assistance in performing the diffraction experiments. We would also like to express our thanks to our colleagues C. Vanpeteghem and M. Guthrie for their assistance with some of the data collection, and J. S. Loveday for help with data analysis. This work was supported by grants from the EPSRC, funding from the CCLRC, and the facilities provided by Daresbury Laboratory. T.B. acknowledges financial support from The Royal Thai Government, Thailand Toray Science Foundation, and The Asahi Glass Foundation.

[1] B. Vasvari, A. O. E. Animalu, and V. Heine, Phys. Rev. **154**, 535 (1967); H. L. Skriver, Phys. Rev. Lett. **49**, 1768 (1982); H. L. Skriver, Phys. Rev. B **31**, 1909 (1985).
[2] M. Hanfland, K. Syassen, N. E. Christensen, and D. L. Novikov, Nature (London) **408**, 184 (2000).
[3] M. Hanfland, I. Loa, and K. Syassen, Phys. Rev. B **65**, 184109 (2002).
[4] R. J. Nelmes, M. I. McMahon, J. S. Loveday, and S. Rekhi, Phys. Rev. Lett. **88**, 155503 (2002).
[5] M. I. McMahon, S. Rekhi, and R. J. Nelmes, Phys. Rev. Lett. **87**, 055501 (2001).
[6] U. Schwarz, A. Grzechnik, K. Syassen, I. Loa, and M. Hanfland, Phys. Rev. Lett. **83**, 4085 (1999).
[7] M. I. McMahon, R. J. Nelmes, and S. Rekhi, Phys. Rev. Lett. **87**, 255502 (2001).
[8] U. Schwarz, K. Takemura, M. Hanfland, and K. Syassen, Phys. Rev. Lett. **81**, 2711 (1998).
[9] D. R. Allan, R. J. Nelmes, M. I. McMahon, S. A. Belmonte, and T. Bovornratanaraks, Rev. High Pressure Sci. Technol. **7**, 236 (1998).
[10] M. I. McMahon, T. Bovornratanaraks, D. R. Allan, S. A. Belmonte, and R. J. Nelmes, Phys. Rev. B **61**, 3135 (2000).
[11] R. J. Nelmes, D. R. Allan, M. I. McMahon, and S. A. Belmonte, Phys. Rev. Lett. **83**, 4081 (1999).
[12] D. M. Adams, High-Pressure Diamond Anvil Cell. Diacell Products, 54 Ash Tree Road, Leicester, U.K.
[13] H. K. Mao, J. Xu, and P. M. Bell, J. Geophys. Res. **91**, 4673 (1986).
[14] R. J. Nelmes and M. I. McMahon, J. Synchrotron Radiat. **1**, 69 (1994).
[15] M. Hanfland, U. Schwarz, K. Syassen, and K. Takemura, Phys. Rev. Lett. **82**, 1197 (1999).

[16] A. P. Hammersley, S. O. Svensson, M. Hanfland, A. N. Fitch, and D. Häusermann, High Press. Res. **14**, 235 (1996).
[17] A. C. Larson and R. B. Von Dreele, Los Alamos National Laboratory Report No. LAUR 860748, 2000.
[18] H. Olijnyk and W. B. Holzapfel, Phys. Lett. **100**, 191 (1984).
[19] M. Winzenick and W. B. Holzapfel, Phys. Rev. B **53**, 2151 (1996).
[20] D. Louër and R. Vargas, J. Appl. Crystallogr. **15**, 542 (1982).
[21] Sr1: $\Delta x=0$; $\Delta y=D$; $\Delta z=0$. Sr2: $\Delta x=-Db\cos(\pi/6)/2a\cos(\beta/2)$; $\Delta y=-D\cos(\pi/3)$; $\Delta z=-Db\cos(\pi/6)/2c\cos(\beta/2)$.
Sr3: $\Delta x=Db\cos(\pi/6)/2a\cos(\beta/2)$; $\Delta y=-D\cos(\pi/3)$; $\Delta z=Db\cos(\pi/6)/2c\cos(\beta/2)$.
[22] Sr1: $\Delta x=-Db/2a\cos(\beta/2)$; $\Delta y=0$; $\Delta z=-Db/2c\cos(\beta/2)$.
Sr2: $\Delta x=Db\cos(\pi/3)/2a\cos(\beta/2)$; $\Delta y=-D\cos(\pi/6)$; $\Delta z=Db\cos(\pi/3)/2c\cos(\beta/2)$.
Sr3: $\Delta x=Db\cos(\pi/3)/2a\cos(\beta/2)$; $\Delta y=D\cos(\pi/6)$; $\Delta z=Db\cos(\pi/3)/2c\cos(\beta/2)$.
[23] Sr1: $\Delta x=-Db\cos(\pi/4)/2a\cos(\beta/2)$; $\Delta y=D\cos(\pi/4)$; $\Delta z=-Db\cos(\pi/4)/2c\cos(\beta/2)$.
Sr2: $\Delta x=-Db\cos(5\pi/12)/2a\cos(\beta/2)$; $\Delta y=-D\cos(\pi/12)$; $\Delta z=-Db\cos(5\pi/12)/2c\cos(\beta/2)$;
Sr3: $\Delta x=Db\cos(\pi/12)/2a\cos(\beta/2)$; $\Delta y=D\cos(5\pi/12)$; $\Delta z=Db\cos(\pi/12)/2\mathrm{c}\cos(\beta/2)$.